Elastic tensor stiffness coefficients for SLS Nylon 12 under different degrees of densification as measured by ultrasonic technique

Antonio Amado-Becker and Jorge Ramos-Grez
Mechanical and Metallurgical Engineering Department, Pontificia Universidad Católica de Chile, Santiago, Chile

María José Yañez and Yolanda Vargas
Physics Department, Universidad de Santiago de Chile, Santiago, Chile, and

Luis Gaete
Ultrasound Laboratory, Santiago, Chile

Abstract

Purpose – The purpose of this paper is to present results of an investigation, where the elastic tensor based on the engineering constants of sinterized Nylon 12 is characterized and is modeled considering a transversely isotropic behavior as a function of apparent density (relative mass density).

Design/methodology/approach – The ultrasound propagation velocity measurement through the material in specific directions by means of the pulse transmission method was used, relating the elastic tensor elements to the phase velocity magnitude through Christoffel's equation. In addition conventional uniaxial tensile tests were carried out to validate the used technique. Laser sintering of Nylon 12 powder (Duraform PA) has been performed at different laser energy densities, fabricating cube-shaped coupons as well as dogbone flat coupons, using an SLS 125 former DTM machine.

Findings – Correlations for each one of the Young moduli, Shear constants and Poisson's ratios, presenting an exponential behavior as a function of the sintering degree, were generated. In addition, as the apparent density reaches a maximum value of 977 kg/m^3 at an energy density of 0.032 J/mm^2, the material behaves in an almost isotropic form, presenting average values for the Young modulus, Shear modulus and Poisson's ratio corresponding to 2,310 MPa, 803 MPa and 0.408, respectively.

Research limitations/implications – The research is limited only to one type of material within the elastic range. Validation of the Young modulus measured along one direction only is performed using a tensile test machine, due to the difficulties in evaluating Poisson's ratios and Shear moduli using conventional tests.

Practical implications – The results presented can be applied to virtual design and evaluating processes such as finite element analysis.

Originality/value – The paper incorporates detailed information regarding the complete elastic characteristics of Nylon 12, including additional measurements of the Shear moduli and Poisson's ratios not studied previously.

Keywords Ultrasonics, Sintering, Tensors, Modulus of elasticity, Polyamides

Paper type Research paper

Introduction

Over the last decade, rapid prototyping (RP) has evolved towards the manufacture of functional prototypes, improving mechanical properties with the aim to integrate end item parts (Agarwala *et al.*, 1995; Das *et al.*, 1998; Wang *et al.*, 2002; Liu *et al.*, 2007). In this direction, the rapid manufacturing concept arises, eliminating the prototype notion when objects with attributes, that satisfy all the final product requirements, are obtained (mechanical resistance, tolerances, superficial roughness, ergonometry, confiability, production costs, etc.). At the present time, RP techniques still do not replace traditional manufacturing methods, fundamentally when high degrees of functionality are requested.

Within the most promising RP technologies for the development of functional prototypes, selective laser sintering (SLS) allows generating complex geometry objects with mechanical properties comparable to conventional methods (Saleh *et al.*, 2004; Kruf *et al.*, 2006; Stein, 2006). Thermoplastic polymers, particularly Nylon 12, have turned out to be adapted for their use in functional parts (Hague *et al.*, 2004). However, functional manufacturing requires complete information

The current issue and full text archive of this journal is available at **www.emeraldinsight.com/1355-2546.htm**

Rapid Prototyping Journal
14/5 (2008) 260–270
 [ISSN 1355-2546]
[DOI 10.1108/13552540810907929]

Received: 7 September 2007
Revised: 25 April 2008
Accepted: 15 May 2008

referring to the mechanical characteristics of sintered materials. This is a preliminary requisite to allow the design under the rapid manufacturing concept. In this sense, several authors (Ajoku *et al.*, 2006b; Caulfield *et al.*, 2006; Zarringhalam *et al.*, 2006) have studied the Nylon 12 elastic mechanical properties in a conventional and not fully complete form, since only the Young modulus based on the build and perpendicular directions has been characterized. Nevertheless, the Nylon 12 elastic tensor characterization has not been performed yet.

Within the available mechanical properties measuring techniques, any type of test performed to a material that does not alter, in a permanent form, its physical, chemical, mechanical or dimensional properties is denominated non-destructive testing. A non-destructive test implies an imperceptible or null damage (Halmshaw, 1991) of the materials integrity.

In the present investigation the non-destructive method by ultrasonic inspection will be used. This technique has been employed in many applications, such as metal crack detection, thicknesses measurements, weld inspections, etc. The motivation for its use in the present investigation is centered in the possibility to characterize the complete elastic properties of the material for each test specimen, eliminating in addition the associated uncertainty using different test samples employed in conventional destructive testing (shear and uniaxial tensile tests), that allow only the partial characterization of the material elastic properties.

In relation to the use of ultrasound for characterization purposes, there is evidence of studies in different materials, showing satisfactory results in relation to measurements obtained by other methods (Wang, 1984; Bucur, 1995; Nielsen and Toftegaard, 2000; Lasaygues and Pithioux, 2002; Najafi *et al.*, 2005; Bucur and Declercq, 2006). However, there are no references that contemplate studies with sintered polymeric materials under this measurement technique.

Background

SLS process parameters

Process parameters are the defined variables that influence and control the SLS process. A number of parameters, some user defined and others defined by geometry or material considerations, affect the quality of parts fabricated. The response of the SLS process is usually described by the geometry and mechanical properties of the object produced. Geometric problems such as curling, shrinkage, growth and poor edge definition and the physical properties such as density, strength and degradation are all influenced by the quantity and timing of energy delivered to the part surface (Williams and Deckard, 1998). The most relevant independent parameters that affect the form the energy is deposited on the powder surface (Figure 1) correspond to the laser power induced on the surface (P), the laser beam spot size (D), the hatch spacing (HS), the beam displacement velocity (V) and the scan line length (L).

These parameters can be related to define expressions that directly describe the energy delivered to the materials surface (Figure 2).

However, the most influential parameters in the SLS process, in terms of geometry accuracy and final mechanical properties of sintered parts, correspond to the power provided by the laser (P) and the beam displacement velocity (V) (Gibson and Shi, 1997; Williams and Deckard, 1998; Yadroitsev *et al.*, 2007). According to this, Nelson (1993) developed a relation to describe the delivered energy incorporating the effect of superposition defined as the fraction of energy density (energy by unit area), also known as the Andrew's number:

Figure 1 SLS independent scanning parameters

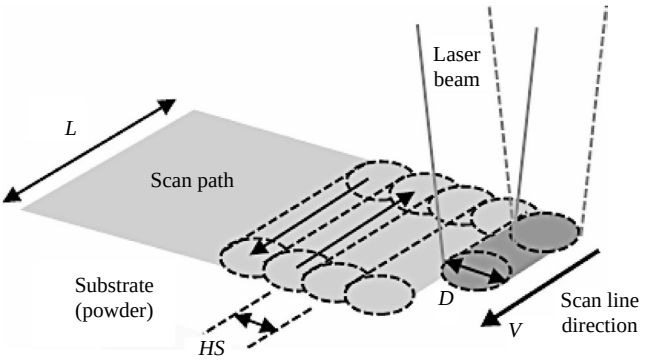

Source: Ramos and Bourell (2003)

$$A_N = \frac{P}{V \cdot HS} \quad (1)$$

At the present time, the Andrew's number is the most used parameter to characterize the energy deposited on the materials surface in terms of the most relevant process variables. For the present investigation, the units employed for this dimensional number are J/mm^2.

Physical model of the SLS materials structure

SLS generates 3D parts in a layer wise manner. In Figure 3 the image of a cross section of the laminated structure of a sintered tensile test specimen (Nylon 12) obtained by means of scanning electron microscopy (SEM) is observed, using a back scattered electron detector.

Observing this structure carefully, it can be distinguished inside of each layer two well-defined structures of distinctive appearance and intimately bonded. The backscattered electron SEM image (Figure 3) shows this layer build up sequence, revealing alternating regions of high- and low-mass density. These two clearly diferenciable structures characterize the laminated behavior, which, in terms of mechanical resistance, allows identifying two main directions: one corresponding to the build axis (perpendicular to the surface lamination), and another direction contained in the lamination plane (perpendicular to the previous direction) (Figure 4).

The mechanical resistance of the material in these two principal directions has been studied by several authors (Ajoku *et al.*, 2006b; Caulfield *et al.*, 2006; Zarringhalam *et al.*, 2006), determining the elastic moduli by means of conventional tensile tests for different energy density levels. However, the information regarding the elastic properties turns out to be incomplete, since the structure given symmetry, can be modeled as a transversely isotropic material. This structure is characterized by a symmetry axis (build axis) through which infinite planes can be drawn. In addition, perpendicular to this direction, the material behaves in an isotropic form (it is represented completely by only two elastic constants). Therefore, the complete characterization of the sintered material is related to a

Figure 2 Relationship between process parameters and energy transferred to the materials surface

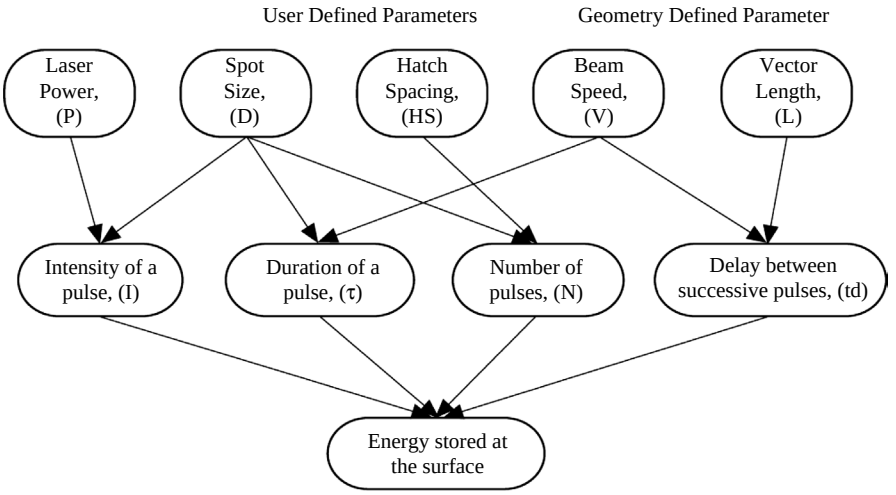

Source: Williams and Deckard (1998)

Figure 3 SEM image of a tensile test specimen cross-section

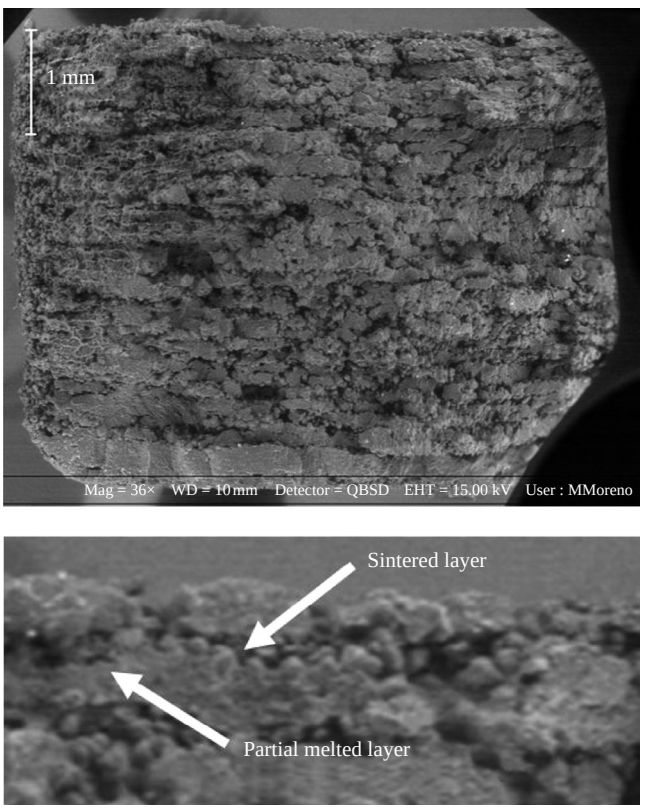

symmetrical effective elastic tensor, which has five independent constants.

Elastic tensor characterization

When dealing with materials such as crystals which possess some degree of symmetry, the Voigt's principle can be applied. This principle states that the symmetry of the physical process is superimposed on the symmetry of the crystal (Nye, 1960). The number of independent elastic constants is therefore reduced as the degree of symmetry

Figure 4 Model for the sintered laminar structure

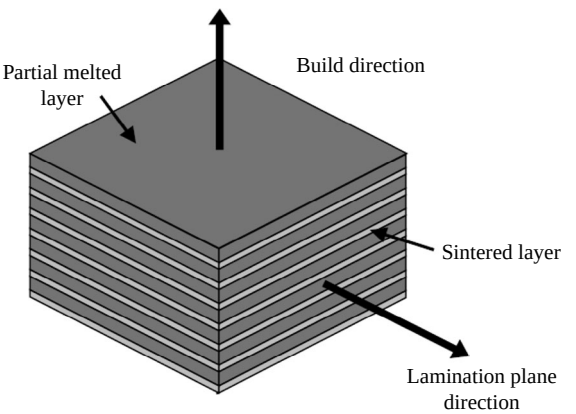

increases. In the present study, the material structure is associated to a hexagonal crystal, which is completely characterized by five independent elastic constants, representing a transversely isotropic behavior. According to the symmetry of this crystal, the notation adopted for the orthogonal main directions is shown in Figure 5.

Figure 5 Principal directions notation

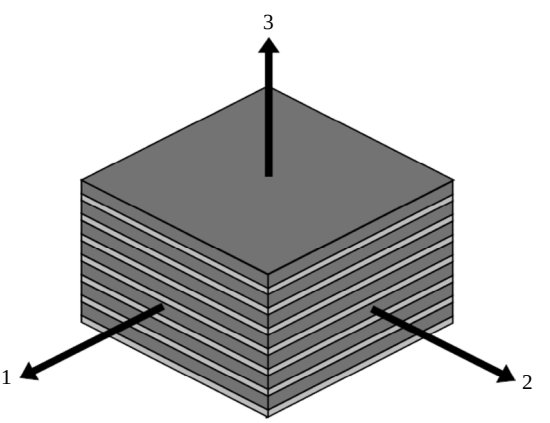

The elastic (stiffness) matrix structure is represented by:

$$\mathbf{C}_{transversely\ \ isotropic} = \begin{bmatrix} C_{11} & C_{12} & C_{13} & 0 & 0 & 0 \\ & C_{11} & C_{13} & 0 & 0 & 0 \\ & & C_{33} & 0 & 0 & 0 \\ & & & C_{44} & 0 & 0 \\ & & & & C_{44} & 0 \\ & & & & & (C_{11}-C_{12})/2 \end{bmatrix} \quad (2)$$

while, the relations between terms of stiffness and compliance matrices (S_{11}, S_{33}, S_{44}, S_{12}, S_{13}) are given by $[\mathbf{C}]^{-1} = [\mathbf{S}]$, where:

$$\mathbf{S}_{transversely\ \ isotropic} = \begin{bmatrix} 1/E_1 & -(\nu_{21}/E_1) & -(\nu_{31}/E_3) & 0 & 0 & 0 \\ -(\nu_{12}/E_1) & 1/E_1 & -(\nu_{31}/E_3) & 0 & 0 & 0 \\ -(\nu_{13}/E_1) & -(\nu_{13}/E_1) & 1/E_3 & 0 & 0 & 0 \\ 0 & 0 & 0 & 1/2\cdot G_{13} & 0 & 0 \\ 0 & 0 & 0 & 0 & 1/2\cdot G_{13} & 0 \\ 0 & 0 & 0 & 0 & 0 & 1/2\cdot G_{11} \end{bmatrix} \quad (3)$$

Given the matrix symmetry, the elements at both sides of the diagonal must be equal, i.e.:

$$\frac{\nu_{13}}{E_1} = \frac{\nu_{31}}{E_3}; \quad \nu_{12} = \nu_{21} \quad (4)$$

Christoffel's equation

In an anisotropic crystal there is often no simple relation between the direction of propagation of a wave and the direction of the particle displacement. In other words, in general the waves are not pure longitudinal or transverse types but are some form of mixed type. There are, however, certain directions in which pure longitudinal and transverse waves may propagate (Pollard, 1977).

For a linear, anisotropic material, Newton's second law and Hooke's law translate into a wave equation of the form:

$$\rho \cdot \frac{\partial^2 u_i}{\partial t^2} = \mathbf{C}_{iklm} \frac{\partial \varepsilon_{lm}}{\partial x_k} \quad (5)$$

where ρ is the density, $\partial^2 u_i/\partial t^2$ the ith component of the volume acceleration, and ε_{lm} is the component of the strain infinitesimal tensor. C_{iklm} is the fourth-rank symmetric stiffness tensor of the material. As mentioned before, if energy considerations are taken into account, C_{iklm} will have only 21 independent components. For the SLS materials microstructure, a hexagonal symmetry is identified, and only five independent elements are determined. In many cases, the elastic wave measurements will rely on plane waves. A plane wave solution to the equation of motion is expressed in terms of the planar displacements specified by $\vec{u}_{(\vec{x},t)}$, which propagate in the direction specified by the unit vector, the wave normal $\vec{n}$. Hence:

$$\vec{u}_{(\vec{x},t)} = A \cdot \vec{p} \cdot \exp(i \cdot (\vec{k} \cdot \vec{x} - \omega \cdot t)) \quad (6)$$

where A is the wave amplitude magnitude and $\vec{p}$ is the polarization vector. Also, $\vec{x}$ represents the position vector, ω the angular frequency of the wave and $\vec{k}$ the wave number vector. Substituting equation (5) into (4) gives for each component:

$$\rho \cdot \omega^2 \cdot u_i = C_{iklm} \cdot k_k \cdot k_l \cdot u_m \quad (7)$$

This equation may be written in a homogeneous form by expressing:

$$u_i = u_m \cdot \delta_{im} \quad (8)$$

where δ_{im} corresponds to the unit tensor. This gives:

$$(C_{iklm} \cdot k_k \cdot k_l - \rho \cdot \omega^2 \delta_{im}) \cdot u_m = 0 \quad (9)$$

Equation (9) was developed by Christoffel (1877) and is now often referred to as Christoffel's equation. It represents a set of three first degree homogeneous equations with u_1, u_2 and u_3 as unknowns. They have non-zero solutions only if the determinant of the coefficients is zero, that is:

$$|C_{iklm} \cdot k_k \cdot k_l - \rho \cdot \omega^2 \delta_{im}| = 0 \quad (10)$$

Alternatively, this expression can be represented in terms of the sound propagation velocity ν (phase velocity), using the following relations:

$$v = \frac{\omega}{k} \quad n_i = \frac{k_i}{k} \quad (11)$$

where n_i corresponds to the director cosines of the normal wave front vector.

Adding the following reduction relation:

$$\lambda_{im} = C_{iklm} \cdot n_k \cdot n_l \quad (12)$$

this gives:

$$|\lambda_{im} - \rho \cdot v^2 \delta_{im}| = 0 \quad (13)$$

Writing this equation out in full:

$$\begin{vmatrix} \lambda_{11} - \rho \cdot v^2 & \lambda_{12} & \lambda_{13} \\ \lambda_{12} & \lambda_{22} - \rho \cdot v^2 & \lambda_{23} \\ \lambda_{13} & \lambda_{23} & \lambda_{33} - \rho \cdot v^2 \end{vmatrix} = 0 \quad (14)$$

Depending on the direction of the propagation vector and according to the crystallographic structure of the stiffness tensor, this expression allows obtaining analytical expressions that relate the elastic tensor elements with the sound propagation velocity in pre-established directions.

In the current study, the five independent constants are completely related to the longitudinal and transverse wave velocities with three propagation directions. These three directions are shown in Figure 6.

Figure 6 Propagation directions of plane waves

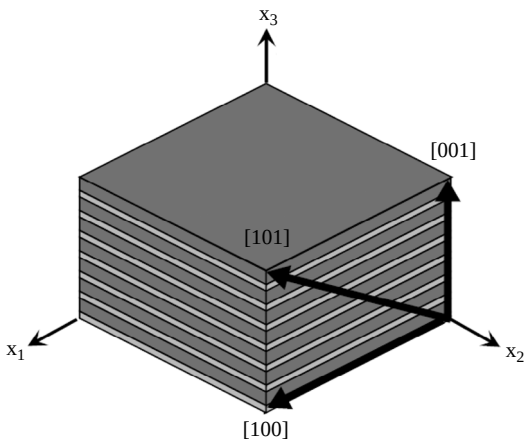

The following expressions relate the stiffness tensor elements with the sound wave propagation velocities:

- *Direction [100]*. The propagation vector is located inside the plane of each layer:

$$v_{\text{Longitudinal}} = \sqrt{\frac{C_{11}}{\rho}}; \quad v_{\text{Transverse1}} = \sqrt{\frac{C_{44}}{\rho}}; \quad v_{\text{Transverse2}} = \sqrt{\frac{C_{11} - C_{12}}{2 \cdot \rho}} \tag{15}$$

  The transverse velocities 1 and 2 have polarization vectors in directions [001] and [010], respectively.
- *Direction [001]*. The propagation vector is perpendicular to each layer, parallel to the x_3 coordinate:

$$v_{\text{Longitudinal}} = \sqrt{\frac{C_{33}}{\rho}}; \quad v_{\text{Transverses1,2}} = \sqrt{\frac{C_{44}}{\rho}} \tag{16}$$

  The transverse velocities 1 and 2 have orthogonal polarization vectors to each other, both located in a plane perpendicular to the longitudinal direction. They may represent any direction inside the plane.
- *Direction [101]*. The propagation vector has an angle of 45° respect to the directions [100] and [001]:

$$v_{\text{Transverse}} = \sqrt{\frac{C_{11} - C_{12} + 2 \cdot C_{44}}{4 \cdot \rho}}$$

$$v_{\substack{\text{Quasi-transverse,} \\ \text{quasi-longitudinal}}} = \sqrt{\frac{\frac{1}{2} \cdot (C_{11} + C_{33} + 2 \cdot C_{44}) \pm \sqrt{\frac{1}{4} \cdot (C_{11} - C_{33})^2 + (C_{13} - C_{44})^2}}{2 \cdot \rho}} \tag{17}$$

  Similar to the previous expressions, two velocities are associated to a transverse direction and one is related to a longitudinal direction, being all orthogonal to each other. However, in this case, the particle displacement (eigenvectors) does not correspond necessarily to perpendicular directions to the propagation axis in the case of transverse waves nor to the movement in the previous direction for the longitudinal case. Since a certain deviation respect to the propagation vector of the orthogonal particle displacement configuration may exist, these velocities receive the quasi-longitudinal and quasi-transverse denomination.

In the case of the first expression of equation (16), analytically it represents a polarization vector in direction [010], corresponding to a transverse displacement. However, this must be verified experimentally.

Experimental setup and procedure

Materials

The sintering equipment employed corresponds to an SLS 125 former DTM series machine. The material used for the specimen sinterization is a Nylon 12 semi-crystalline thermoplastic polymer powder, known as Duraform PA polyamide (3DSystems). The principal thermal and mechanical properties are summarized in Table I.

Experimental design

A total of six specimen sets were sintered. For each one of them a different energy density was used, considering only the laser beam power variation shown in Table II.

The other process parameters remained constant, with values corresponding to a hatch spacing of 0.15 mm with laser beam superposition (beam spot size of 0.45 mm) and a scan line velocity of 1,636 mm/s. The height of each layer was set at a fixed value of 0.10 mm. In relation to the Andrew's number, the energy densities applied over the powder surface are presented in Table III.

For the ultrasound measurement tests, six cube shaped specimens for each energy density level were considered. In a similar way, for the uniaxial tensile test, three dogbone flat coupons for a same level were sintered. The geometry of each test sample was considered according to the ASTM (2003) D638-3 and ASTM (2001) E494-95 standard norms for the uniaxial tensile test and ultrasound specimens, respectively. The shape and dimensions of each one of them is shown in Figure 7.

Table I Nylon 12 Duraform PA principal properties

Particle shape	**Irregular**
Particle size, range 90 percent	25-92 μm
Average particle size	58 μm
Maximum density (injection molded)	1,030 kg/m^3
Melting temperature	186°C

Sources: Tontowi and Childs (2001) and Ajoku *et al.* (2006a, b)

Table II Laser power values applied

Set	**1**	**2**	**3**	**4**	**5**	**6**
Power (*W*)	3.00	4.00	5.00	5.75	6.00	8.00

Table III Energy density values applied

Set	**1**	**2**	**3**	**4**	**5**	**6**
Energy density (J/mm^2)	0.012	0.016	0.020	0.023	0.024	0.032

Figure 7 Cube shaped coupon (a) and dogbone flat coupon (b)

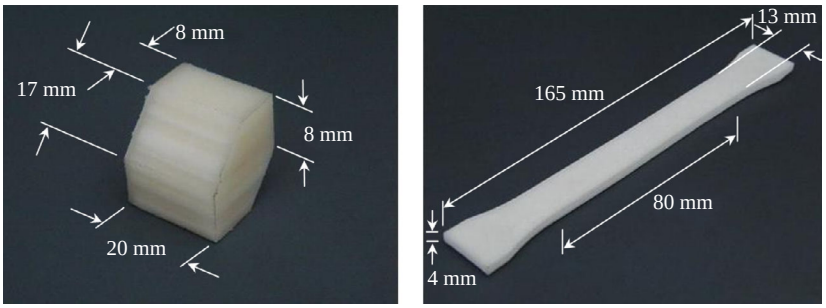

In addition, the sintered test coupons set orientation over the part piston surface is shown in Figure 8.

Method

The ultrasonic through-transmission method was used to measure the ultrasonic wave velocity of bulk waves (longitudinal and shear waves) in principal symmetry axes and at 45° to symmetry directions 1 and 2 as shown in Figure 6. This method consists of locating an emitting ultrasonic transducer at one end of the sample and a receiving transducer at the other, as shown in Figure 9 (see details in Figure 10).

The central frequencies of the broad band transducers were 1 MHz for both longitudinal and shear waves (Panametrics part no. V152). For coupling the longitudinal transducers to the test samples solid petroleum jelly was used. In case of the shear transducers, a Panametrics SWC couplant was employed. Also, the transducers were positioned in a specially designed support to exert a constant pressure on the samples faces, maintaining the alignment of the communications axis signal. The ultrasonic device employed was a Panametrics 5077 PR pulser/receiver system. The signal received by the receiving transducer was unfolded in the Tie-Pie 801 oscilloscope with a precision of 20 ns, incorporated with the computer.

The wave propagation velocity was calculated by measuring the time of flight. It consists of measuring the signal transmission time t_v through the sample, considering the arrival time corresponding to the first signal maximum or "peak" (curved line shown on the computer screen

Figure 8 Test coupons set orientation over the part piston surface

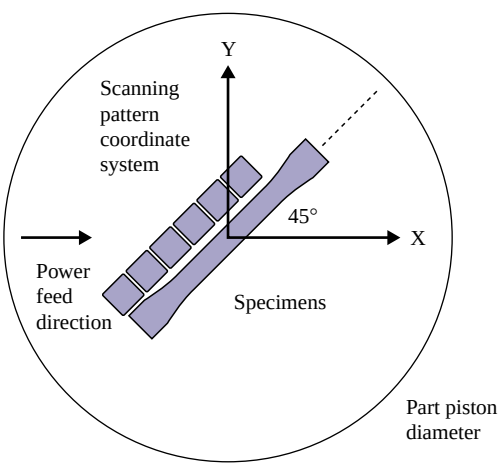

Figure 9 Experimental setup for ultrasonic propagation velocity measurements

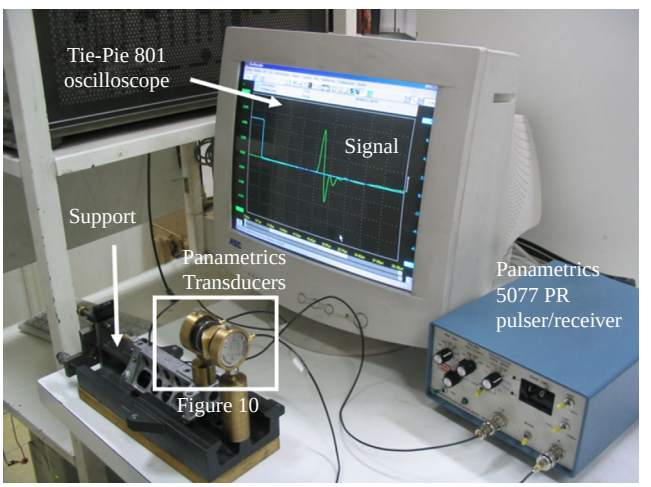

Figure 10 Ultrasonic shear wave measurement setup

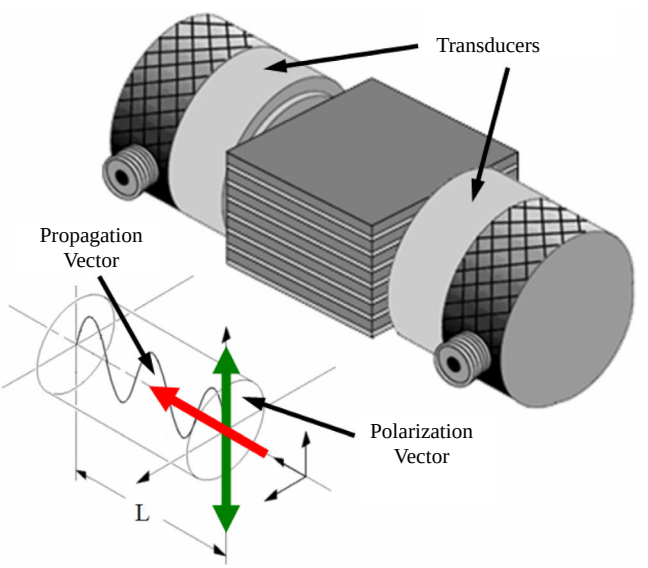

in Figure 9). In addition, the transducers delay time t_r was registered. Then, using the samples length l for a particular direction between parallel faces, the wave velocity can be calculated as follows:

$$v_p = \frac{l}{t_v - t_r} \tag{18}$$

For each wave propagation direction (principal symmetry axes), one longitudinal and two transverse velocities with orthogonal polarization vectors were registered. Moreover, measurements of two additional transverse velocities with orthogonal polarization vectors were made in the diagonal direction of the cube face 2 (Figure 6). Finally, each measurement was made twice, with the aim to register possible dispersions. In summary, 792 independent wave propagation velocity measurements were carried out (three longitudinal and eight transverse per sample). In addition, uniaxial tensile tests (ASTM D638-3) were also performed along direction 1 to compare and validate part of the results.

Finally, apparent density was obtained from the ultrasonic coupons. It was calculated using the weighed mass divided by measured volume for each on of the specimens. A Scherr-Tumico Vernier caliper for length measurements was used and an A&D Gemini GR-202 precision balance was employed.

Results and discussion

SLS materials apparent density

From Figure 11 as the energy density increases, the densification degree of the sintered material also increases. The behavior is characterized by an inflection point, from which the rate of densification decreases, reaching a maximum density value equivalent to 977 kg/m^3, which never overcomes the 1,030 kg/m^3, corresponding to the maximum mass density reported for injection molded Nylon 12 (Ajoku *et al.*, 2006a). The change in the densification rate for this material also has been validated experimentally and by numerical simulations in other studies, obtaining similar results (Tontowi and Childs, 2001). This curvature change is attributable to the predominance of a particle union by a mechanism of fusion instead of a viscous sintering phenomenon. It is important to mention that when comparing this curve with the one reported by Caulfield *et al.* (2006), it can be observed that a peak occurs just before the last density point. As explained by Caulfield *et al.* (2006), this may be attributed to the powder particles becoming damaged or burnt by excess heat from the laser beam, causing a degradation of the material above a certain energy density threshold.

Figure 11 Mass density as a function of energy density

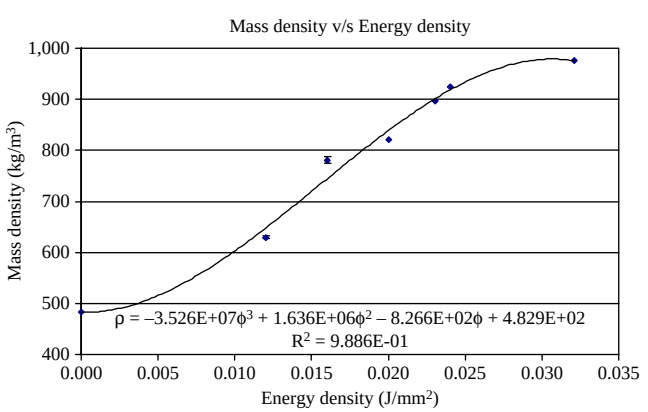

Wave propagation velocity

As the materials apparent density is increased, the longitudinal propagation velocity is raised, too (Figure 12). The longitudinal velocities in directions 1 and 2 turn out to be equal in magnitude for each densification degree. The similarity between these magnitudes verifies a necessary condition for the transversely isotropic characterization, corresponding to the axis-symmetry of the sintering plane along the x_3 coordinate. The propagation velocity in the direction perpendicular to the lamination plane presents a similar behavior, but being lower in magnitude. The authors believed this could be attributed to small fluctuations in mass density within each sintered layer. As the disturbance crosses a region of low-mass density, there is less cohesion in between particles, due the combined effect of a reduction in the binding force between particles and a rigidity loss within these unions (small "necks").

Similar to the longitudinal propagation velocities, as the materials apparent density is increased, it also increases the transverse sound wave propagation velocity. However, in this case, the behavior of the densification degree appears to be linear. In addition, the magnitude of each pair of velocities (Figures 13-16) practically turns out to be equal, which is an additional necessary condition for the characterization of the material according to a transversely isotropic behavior as it has been assumed initially. Comparing the curve fitting behavior for both types of wave (longitudinal and transverse), as each transverse propagation velocity is correlated proportionally to the elastic tension terms, the disturbances associated to shear elastic deformations would present a lower sensitivity level based on the sintering degree due their linear behavior.

The results of the transverse velocity along the propagation direction, corresponding to the diagonal of the cube lateral faces (face 2), are shown in Figure 16. Two transverse velocities with the same wave propagation direction, but with orthogonal polarization vectors are shown, where each one of them is associated to directions $[\bar{1}01]$ and [010], respectively. Although infinite polarization vectors can be drawn up, any one of them is located between the two previous orthogonal directions. Owing to the physical characteristics of the propagation wave phenomenon, it would not be probable that an orientation between these two directions can generate a considerably different propagation velocity magnitude far away from the measured values. On the basis of this

Figure 12 Longitudinal velocities as a function of the sintering degree

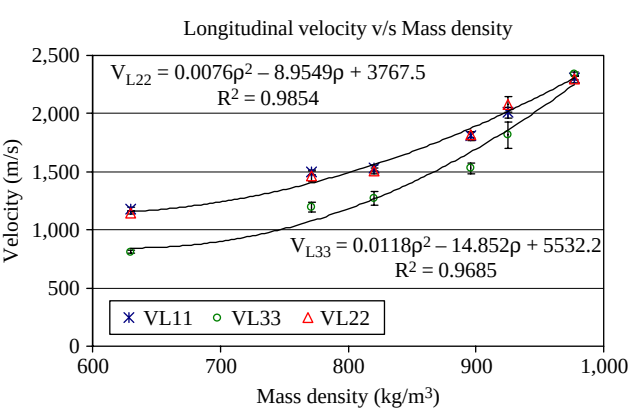

Figure 13 Transverse velocities with propagation and polarization vectors contained inside the lamination plane

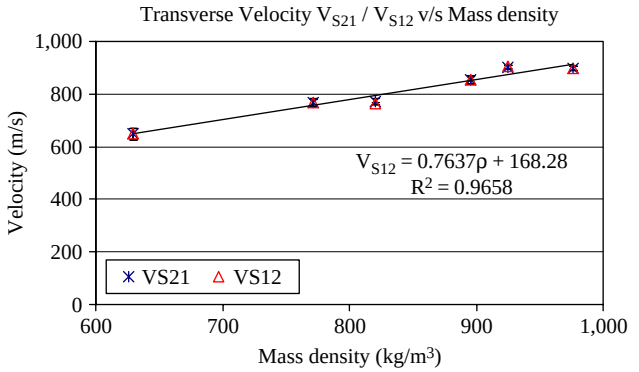

Figure 14 Transverse velocities with propagation vector contained inside the lamination plane and perpendicular to the polarization vector

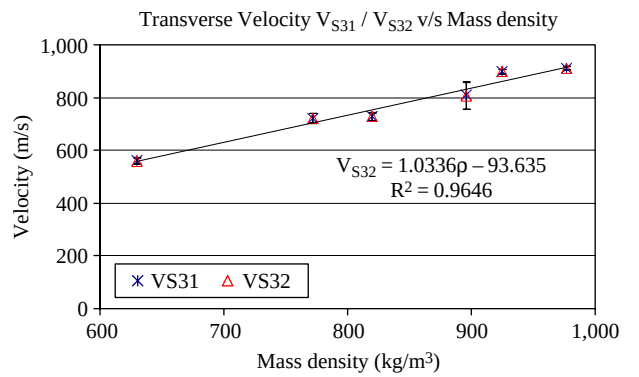

Figure 15 Transverse velocities with polarization vector contained inside the lamination plane and perpendicular to the propagation vector

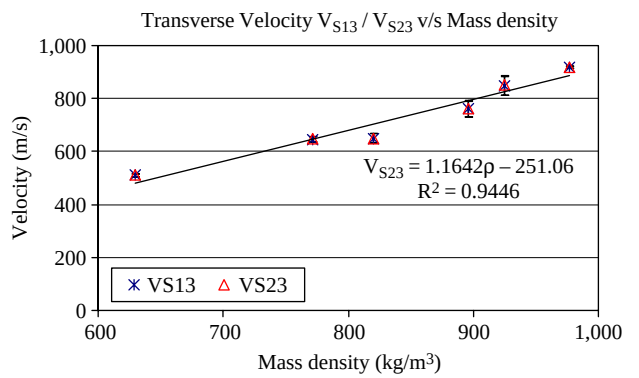

argument, and as it is shown in Figure 16, both velocities practically seem to be equal. In addition, when comparing the magnitude of $V_{dS[010]}$ measured experimentally with the calculated one by means of the first expression of equation (17), it can be verified that both agree, since they present an average magnitude difference for each sintering degree lower than 5 percent. In relation to this consideration, it can be assumed that the quasi-transverse velocity would correspond to a very similar value. So, if this result is used to evaluate the second expression of equation (17), the C_{13}

Figure 16 Transverse velocities with propagation vector in diagonal direction

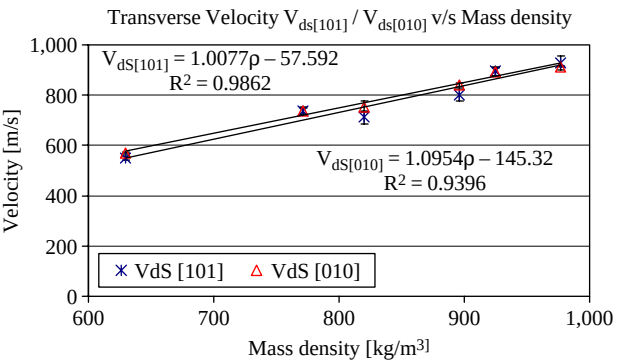

element associated to the stiffness tensor can be determined. However, a final verification with conventional uniaxial tensile tests is performed to validate the proposed argument.

Engineering elastic constants

The behavior of the engineering elastic constants as a function of the sintering degree is shown in Figures 17 and 18.

As the apparent density of the material is incremented, the value of each one of the elastic constants belonging to the stiffness tensor increases. In the first graph, tensile and shear moduli are correlated by means of an exponential function. The Young's modulus in direction 1 (perpendicular lamination direction) turns out to be greater than the Young's modulus in direction 3 (lamination direction) within the complete materials apparent density range in study. This difference between the tensile moduli can be explained because of the low resistance to deformation that direction 3 presents, most likely due to fluctuations in mass density. As it was mentioned previously, inside each layer there are particles that have adhered to each other with different sintering degrees, which means local variations of the joint stiffness (necks). The net effect of these local variations generates the lower value of the tensile moduli along the build direction. However, as the densification degree increases, both curves converge to a maximum common average value for the Young's modulus corresponding approximately to 2,310 MPa, when mass density reaches 977 kg/m^3. The same behavior is

Figure 17 Elastic moduli as a function of the sintering degree

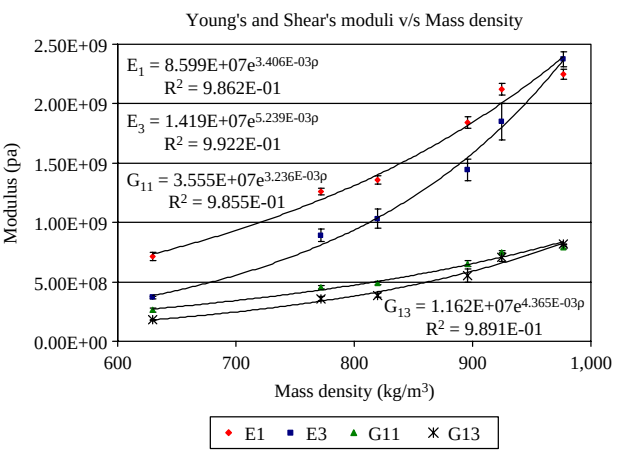

Figure 18 Poisson's ratios as a function of the sintering degree

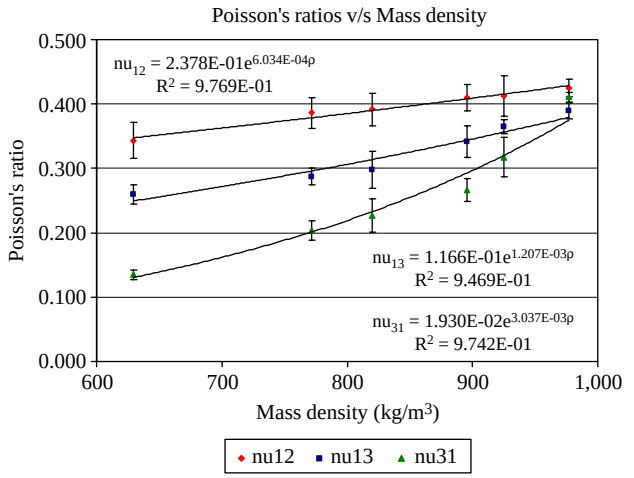

observed when considering the curves corresponding to the Shear's moduli, with a common value of 803 MPa at the same sintering degree. According to the literature, the maximum value for the sintered Nylon 12 Young's modulus is not reported exactly, presenting a broad dispersion of values that vary from 1,100 to 2,050 MPa (Ajoku *et al.*, 2006b; Caulfield *et al.*, 2006; Zarringhalam *et al.*, 2006). Although the maximum value determined by the ultrasonic technique is higher than those measured, its validation is verified by means of conventional uniaxial tensile test for direction 1 (Figure 19).

The agreement between both results is quite acceptable, presenting a maximum difference of 13 percent for the lower sintering degree. For higher densification levels, this percentage difference is lower than 10 percent.

Analyzing the convergence of all engineering constants, it can be established that, as the apparent density is incremented, the material would behave in a homogenous form towards any direction, almost similar to an isotropic material. In order to verify this argument, in any material with isotropic behavior the determination of the third constant can be obtained based on the remaining two constants, through the following relation:

Figure 19 Comparison of the Young's modulus along the laminar direction as a function of the sintering degree

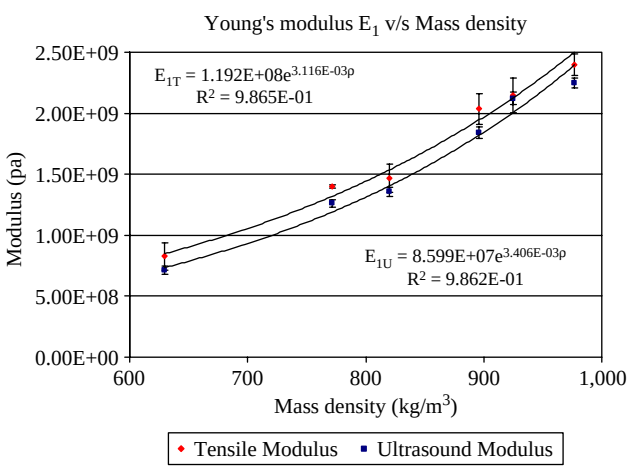

$$G = \frac{E}{2 \cdot (1 + \nu)} \tag{19}$$

Replacing the average values for the highest density achieved:

$$G = \frac{2,310}{2 \cdot (1 + 0.408)} = 820\,\text{MPa} \tag{20}$$

The Shear's modulus obtained considering Christoffel's relations corresponds to a value of 803 MPa, which approximately represents a difference of 2 percent, validating the argument of an isotropic behavior tendency with the densification increase.

On the other hand, also it is possible to express the previous results based on the applied energy density, as it is shown in Figures 20 and 21, using the obtained regression shown in Figure 11.

Conclusions

From each tensor, measured at each apparent density, exponential correlations for the Young's moduli, Shear's moduli and Poisson's ratios as function of the sintering degree have been calculated from ultrasonic technique measurements, signaling an increasing and converging trend of the mechanical properties with increasing energy density, towards those of an isotropic material at the maximum achieved powder density. Average values for Nylon 12 isotropic elastic constants corresponded to 2,310 MPa,

Figure 20 Elastic moduli as a function of the energy density

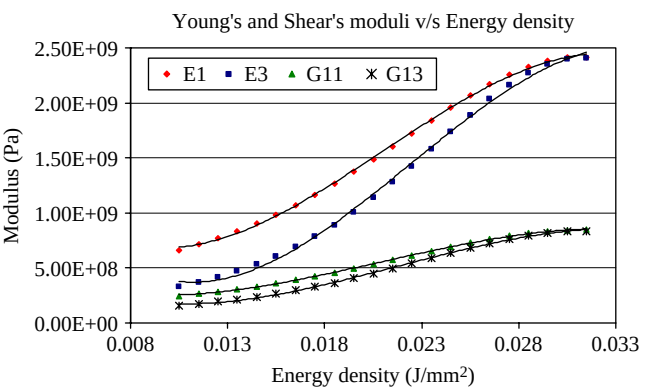

Figure 21 Poisson's ratios as a function of the energy density

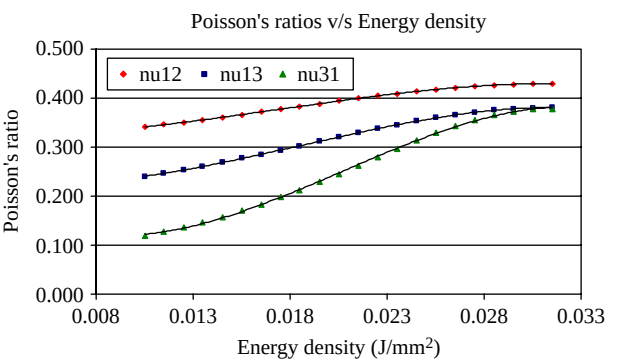

803 MPa and 0.408 for the Young's modulus, Shear's modulus and Poisson's ratio, respectively. These values are obtained for a maximum apparent density (mass density) equivalent to 977 kg/m^3. Uniaxial tensile tests were also performed on the laser sintered dogbone coupons to compare the two characterization techniques, indicating that a good agreement exits between them, at least for the measurements of the Young's modulus along the dogbone axis (~2.4 GPa).

Finally, ultrasonic technique is very versatile providing results that otherwise would have been difficult to measure and which moreover have helped validating tensile test results. The latter, suggests this technique could provide the rapid manufacturing industry with a suitable non-destructive testing technique, allowing accurate determination of the mechanical properties of the resulting materials from such advanced manufacturing processes.

References

Agarwala, M., Bourell, D., Beaman, J., Marcus, H. and Barlow, J. (1995), "Post-processing of selective laser sintered metal parts", *Rapid Prototyping Journal*, Vol. 1 No. 2, pp. 36-44.

Ajoku, U., Hopkinson, N. and Caine, M. (2006a), "Experimental measurement and finite element modelling of the compressive properties of laser sintered Nylon-12", *Materials Science and Engineering: A*, Vol. 428 Nos 1/2, pp. 211-6.

Ajoku, U., Saleh, N., Hopkinson, N., Hague, R. and Erasenthiran, P. (2006b), "Investigating mechanical anisotropy and end-of-vector effect in laser-sintered nylon parts", *Proceedings of the Institution of Mechanical Engineers, Part B: Journal of Engineering Manufacture*, Vol. 220 No. 7, pp. 1077-86.

ASTM (2001), *Annual Book of ASTM Standards*, American Society for Testing and Materials, West Conshohocken, PA, Standard E494-95 practice for measuring ultrasonic velocity in materials.

ASTM (2003), "Standard D638-03 test method for tensile properties of plastics", *Annual Book of ASTM Standards*, American Society for Testing and Materials, West Conshohocken, PA.

Bucur, V. (1995), *Acoustics of Wood*, 1st ed., CRC Press, Salem, MA.

Bucur, V. and Declercq, N.F. (2006), "The anisotropy of biological composites studied with ultrasonic technique", *Ultrasonics*, Vol. 44 No. 1, pp. e829-31.

Caulfield, B., McHugh, P.E. and Lohfeld, S. (2006), "Dependence of mechanical properties of polyamide components on build parameters in the SLS process", *Journal of Materials Processing Technology*, Vol. 183 Nos 1/3, pp. 477-88.

Christoffel, E. (1877), "B. Ann. di Mat. (Ser. 2)", t. 8, reprinted in *Ges. Math. Abhandlungen*, Vol. 2, Brockhaus, Leipzig, 1910, p. 81.

Das, S., Beaman, J.J., Wohlert, M. and Bourell, D.L. (1998), "Direct laser freeform fabrication of high performance metal components", *Rapid Prototyping Journal*, Vol. 4 No. 3, pp. 112-17.

Gibson, I. and Shi, D. (1997), "Material properties and fabrication parameters in selective laser sintering process", *Rapid Prototyping Journal*, Vol. 3 No. 4, pp. 129-36.

Hague, R., Mansour, S. and Saleh, N. (2004), "Material and design considerations for rapid manufacturing", *International Journal of Production Research*, Vol. 42 No. 22, pp. 4691-708.

Halmshaw, R. (1991), *Non-destructive Testing*, 2nd ed., Arnold Publishers, London.

Kruf, W., van de Vorst, B., Maalderink, H. and Kamperman, N. (2006), "Design for rapid manufacturing functional SLS parts", *Innovative Production Machines and Systems Virtual Conference*, available at: http://conference.iproms.org/design_for_ rapid_manufacturing_functional_sl-s_parts (accessed July 10, 2007)

Lasaygues, P. and Pithioux, M. (2002), "Ultrasonic characterization of orthotropic elastic bovine bones", *Ultrasonics*, Vol. 39 No. 8, pp. 567-73.

Liu, J.H., Shi, Y.S., Lu, Z.L., Xu, Y., Chen, K.H. and Huang, S.H. (2007), "Manufacturing metal parts via indirect SLS of composite elemental powders", *Materials Science and Engineering: A*, Vol. 444 Nos 1/2, pp. 146-52.

Najafi, S.K., Bucur, V. and Ebrahimi, G. (2005), "Elastic constants of particleboard with ultrasonic technique", *Materials Letters*, Vol. 59, pp. 2039-42.

Nelson, J.C. (1993), "Selective laser sintering: a definition of the process and an empirical sintering model", PhD thesis, University of Texas, Austin, TX.

Nielsen, S.A. and Toftegaard, H. (2000), "Ultrasonic measurement of elastic constants in fiber-reinforced polymer composites under influence of absorbed moisture", *Ultrasonics*, Vol. 38 Nos 1/8, pp. 242-6.

Nye, J.F. (1960), *Physical Properties of Crystals: Their Representation by Tensors and Matrices*, 2nd ed., Oxford University Press, Oxford.

Pollard, H.F. (1977), *Sound Waves in Solids*, 1st ed., Pion Limited, London.

Ramos, J.A. and Bourell, D.L. (2003), "Mechanics of the selective laser raster-scanning surface interaction", *Proceedings of the 14th Solid Freeform Fabrication Symposium Austin, TX*, pp. 559-72.

Saleh, N., Hopkinson, N., Hague, R. and Wise, S. (2004), "Effects of electroplating on the mechanical properties of stereolithography and laser sintered parts", *Rapid Prototyping Journal*, Vol. 10 No. 5, pp. 305-15.

Stein, G.N. (2006), "Development of high-density nylon using direct manufacturing/selective laser sintering", *Northrop Grumman Technology Review Journal*, Vol. 14 No. 2, pp. 67-79.

Tontowi, A.E. and Childs, T.H.C. (2001), "Density prediction of crystalline polymer sintered parts at various powder bed temperatures", *Rapid Prototyping Journal*, Vol. 7 No. 3, pp. 180-4.

Wang, J.C. (1984), "Young's modulus of porous materials", *Journal of Materials Science*, Vol. 19 No. 3, pp. 801-8.

Wang, X.C., Laoui, T., Bonse, J., Kruth, J.P., Lauwers, B. and Froyen, L. (2002), "Direct selective laser sintering of hard metal powders: experimental study and simulation", *The International Journal of Advanced Manufacturing Technology*, Vol. 19 No. 5, pp. 351-7.

Williams, J.D. and Deckard, C.R. (1998), "Advances in modeling the effects of selected parameters on the SLS

process", *Rapid Prototyping Journal*, Vol. 4 No. 2, pp. 90-100.
Yadroitsev, I., Bertrand, P. and Sumurov, I. (2007), "Parametric analysis of the selective laser melting process", *Applied Surface Science*, Vol. 253 No. 19, pp. 8064-9.
Zarringhalam, H., Hopkinson, N., Kamperman, N.F. and de Vlieger, J.J. (2006), "Effects of processing on microstructure and properties of SLS Nylon 12", *Materials Science and Engineering: A*, Vol. 435-436 No. 5, pp. 172-80.

Corresponding author

Jorge Ramos-Grez can be contacted at: jramos@ing.puc.cl